DOI: 10.1002/ejic.200900515

Ferrocene-Substituted [Mn_4] Dicubane Single-Molecule Magnets

Katie J. Heroux,[a] Arnold L. Rheingold,[a] and David N. Hendrickson*[a]

Keywords: Ferrocene / Magnetic properties / Magnetoanisotropy / Manganese / Oxidation / Single-molecule magnet

Two new mixed-valent [Mn_4] single-molecule magnets (SMMs) have been synthesized by using *N*-alkylated diethanolamine ligands and ferrocenecarboxylic acid. Both complexes exhibit weak ferromagnetic exchange and appreciable axial zero-field splitting as evidenced by DC magnetic susceptibility and field-dependent magnetization measurements. A significant frequency-dependent out-of-phase signal in the AC susceptibility is also observed for both complexes, a feature that is characteristic of SMMs. The ground-state spin of each complex was determined from the DC data and extrapolation of the low-frequency AC data, giving a value of S = 8. This result is consistent with the previously reported and structurally similar S = 8 and S = 9 [Mn_4] dicubane SMMs.

Introduction

Single-molecule magnets are polynuclear metal clusters that exhibit a large spin ground state and an appreciable magnetoanisotropy. Together, these characteristics give rise to a potential energy barrier between the "spin up" and "spin down" orientations of the magnetic moment, leading to phenomena such as slow magnetization relaxation, magnetization hysteresis, and quantum tunnelling of the magnetization (QTM).[1] SMMs are ideal candidates for high-density storage devices and quantum computing because they are monodisperse in size, shape, spin, and orientation in their crystalline state. However, quantum tunneling must occur coherently between the "spin up" and "spin down" energy wells if such applications are ever to be fully realized. Several environmental factors such as phonon effects, nuclear spins, and intermolecular interactions contribute significantly to decoherence in SMMs.[2] Thus, there has been much effort directed at designing systems with minimal environmental coupling in order to achieve quantum coherence.

One approach to this problem is to limit the intermolecular interactions between neighboring molecules in the crystal lattice by using bulky peripheral ligands to provide "insulation" around the magnetic core. This method has proven to be effective in reducing intermolecular interactions in tetranuclear Ni^{II} SMMs as evidenced by the near elimination of an exchange bias in the hysteresis loops.[3] As first recognized in an antiferromagnetically coupled dimer of [Mn_4] cubane SMMs, exchange-biased quantum tunneling can have dramatic effects on the magnetic and quantum properties of an SMM.[4] Another strategy is to synthesize highly charged SMMs which can then be isolated by bulky counterions. The ability to then vary the counterion will provide another avenue to further tune the structural and magnetic properties of SMMs.

With these goals in mind, the ferrocenecarboxylate $(FcCO_2)^-$ ligand was an attractive candidate for several reasons. The ferrocene substituent alone will provide some steric hindrance to the cluster which may lead to interesting structural and magnetic properties. Furthermore, a cationic SMM could potentially be synthesized by taking advantage of the redox properties of ferrocene. The resulting ferrocenium (Fc^+) analog will have added electrostatic bulk and also allow for the incorporation of large anions such as BPh_4^- to further isolate the SMMs. Masello et al.[5] recently reported a family of Mn clusters containing ferrocene-1,1′-dicarboxylate ligands with the intention of eventually studying the Fc^+ analogs. However, although all of the clusters exhibit non-zero ground-state spins, none appear to be SMMs.

Herein we report the synthesis of two ferrocene-substituted [Mn_4] dicubanes along with their structural and magnetic characterization. *N*-Alkylated diethanolamine ligands ($RdeaH_2$) are widely used in the synthesis of [Mn_4] dicubanes, as well as higher nuclearity SMMs, for their structural flexibility and tunable nature of the alkyl substituent.[6,7] In fact, the two complexes discussed here can be closely compared to their S = 9 benzoate analogs, $[Mn^{II}_2Mn^{III}_2(O_2CPh)_4(Mdea)_2(MdeaH)_2]\cdot CH_2Cl_2\cdot Et_2O$ and $[Mn^{II}_2Mn^{III}_2(O_2CPh)_4(Bdea)_2(BdeaH)_2]$, though the latter was synthesized by a vastly different procedure using μ_3-oxo-centered Fe triangles as the carboxylate source.[8,9]

[a] Department of Chemistry and Biochemistry, University of California at San Diego,
9500 Gilman Dr., La Jolla, CA 92093, USA
Fax: +1-858-534-5383
E-mail: dhendrickson@ucsd.edu
Supporting information for this article is available on the WWW under http://dx.doi.org/10.1002/ejic.200900515.

Results and Discussion

The complexes $[Mn^{II}_2Mn^{III}_2(O_2CFc)_4(Mdea)_2(MdeaH)_2 \cdot 4MeCN]$ (**1**) and $[Mn^{II}_2Mn^{III}_2(O_2CFc)_4(Bdea)_2(BdeaH)_2] \cdot 2MeCN$ (**2**) were synthesized by the reaction of Mn^{II} acetate and ferrocenecarboxylic acid ($FcCO_2H$) in MeCN with an excess of triethylamine. The corresponding *N*-alkylated diethanolamine, *N*-methyldiethanolamine ($MdeaH_2$) for **1** and *N*-butyldiethanolamine ($BdeaH_2$) for **2**, was added to a stirred solution, which was then refluxed for 1 h. Brown plate-like single crystals for X-ray diffraction were obtained by diethyl ether diffusion of the MeCN solution. Though both complexes contain co-crystallized MeCN solvate molecules, elemental analysis confirms that samples prepared for magnetic studies were desolvated.

In the absence of the bulky ferrocene ligand, similar reactions (with only smaller carboxylates present like acetate, propionate, or butyrate) result in higher nuclearity wheel-shaped Mn SMMs such as the $[Mn_{12}]$ and $[Mn_{16}]$ wheels reported by Shah et al.[7,10] Therefore, the resulting topology of **1** and **2** is speculated to be strongly influenced by the steric effects of the larger ferrocenecarboxylate ligand, similar to the benzoate-substituted case.[8]

Complexes **1** and **2** both crystallize in the $P\bar{1}$ space group with two halves of the molecule related by inversion symmetry. There is a single orientation of the $[Mn_4]$ structure in the unit cell. An ORTEP of **2** is shown in Figure 1 whereas that of **1** (nearly isostructural) can be found in Figure S1 in the Supporting Information (crystallographic data and refinement parameters for **1** and **2** are summarized in Table S1). Both complexes comprise an $[Mn^{II}_2Mn^{III}_2O_6]^{4+}$ double-cuboidal core with two heptacoordinate distorted pentagonal-bipyramidal Mn^{II} ions, Mn(1), at the wing positions and two hexacoordinate pseudo-octahedral Mn^{III} ions, Mn(2), at the body positions. The oxidation states of the Mn ions were determined by charge considerations, the presence of Jahn–Teller distortion around the high-spin Mn^{III} ions, and bond valence sum analyses (Table S2). Also, this pseudo-dicubane mixed-valent core is a well-known topology for Mn SMMs.

The coordination sphere of the Mn^{III} ions consists of an apical N-atom from the doubly deprotonated *N*-alkyldiethanolamine ligand, two μ_3- and two μ_2-alkoxy arms of the amine ligands, and an oxygen atom of a bridging (Mn^{II}–Mn^{III}) ferrocenecarboxylate monoanion. For the Mn^{II} ions, the singly deprotonated tridentate *N*-alkylated diethanolamine occupies three positions in the pentagonal plane. The other equatorial positions are occupied by a μ_3-alkoxide of the other amine ligand and an oxygen atom of the bridging ferrocenecarboxylate. The monodentate ferrocenecarboxylate coordinates to the Mn^{II} ion via a single oxygen atom in an apical position. A μ_2-alkoxide arm in the other axial coordination site completes the coordination sphere of the Mn^{II} ions.

The direct-current (DC) magnetic susceptibility of **1** and **2** in an applied field of 0.1 T and a temperature range of 300–1.8 K can be found in Figure 2. As can be seen from the data, $\chi_M T$ gradually increases as the temperature is lowered from 300 K, indicative of intramolecular ferromagnetic exchange. A maximum $\chi_M T$ value of 26.5 $cm^3 mol^{-1} K$ (at 1.8 K) and 33.9 $cm^3 mol^{-1} K$ (at 3.8 K) is reached for **1** and **2**, respectively. Because there are only two dominant exchange pathways (J_{bb} between the Mn^{III} ions and J_{wb} between the Mn^{II} and Mn^{III} ions) based on the inversion symmetry of the $[Mn_4]$ core, the Kambe vector coupling method was employed to derive an appropriate spin Hamiltonian (see Supporting Information).

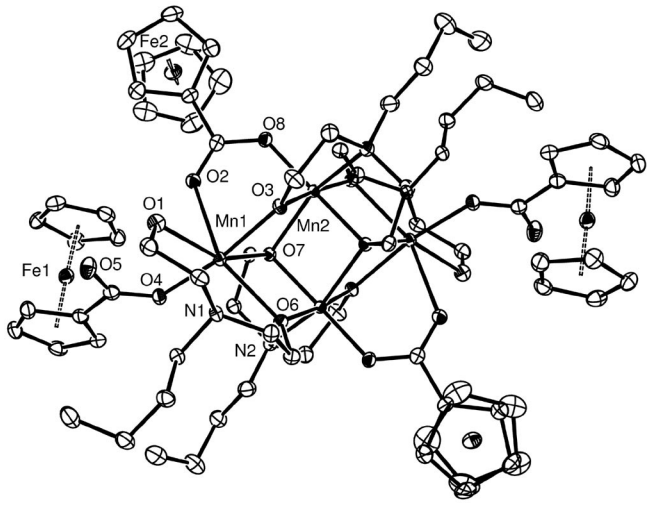

Figure 1. ORTEP of **2** with hydrogen atoms omitted for clarity and thermal ellipsoids at 50% probability level.

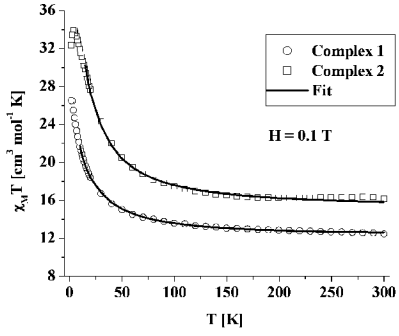

Figure 2. $\chi_M T$ vs. T at an applied magnetic field of 0.1 T for **1** and **2**.

The resulting eigenvalue expression along with the corresponding Van Vleck equation was then used to least-squares-fit the experimental data (solid lines in Figure 2). Reasonable fits were obtained from 300 to 15 K with final optimized parameters of g = 1.8, J_{wb} = 0.18 cm^{-1}, J_{bb} = 2.3 cm^{-1} for **1** and g = 2.0, J_{wb} = 0.44 cm^{-1}, J_{bb} = 2.4 cm^{-1} for **2**. The fits for both complexes indicate a poorly isolated ground-state spin of S = 9 with a low-lying first excited state of S = 8 (only 1.7 cm^{-1} and 4.4 cm^{-1} above the ground state for **1** and **2**, respectively).

To confirm the ground-state spin and determine the magnitude of the zero-field splitting parameter, D, field-dependent magnetization measurements were also made at applied

fields of 5, 4, 3, 2, and 1 T in the 4–1.8 K temperature range. The data for **1** (Figure S2) and **2** (Figure 3) are plotted as reduced magnetization $M/N_{\mu B}$ vs. H/T, where M is the magnetization, N is Avogadro's number, μ_B is the Bohr magneton, and H is the magnetic field. The data were least-squares-fit to a spin Hamiltonian including an isotropic Zeeman interaction and an axial zero-field splitting parameter (DS_z^2).

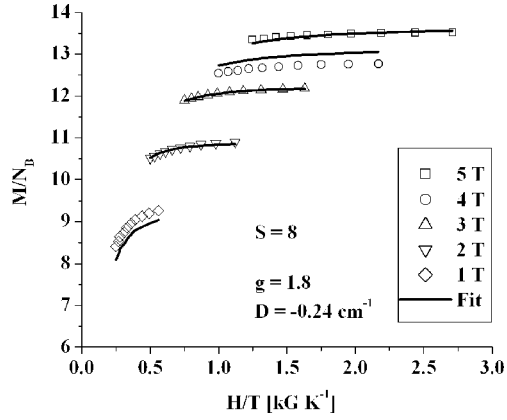

Figure 3. Field-dependence of the magnetization for **2**.

The best fits for the reduced magnetization of **1** and **2** (solid lines in the respective figures) were found by assuming an S = 7 ground state (g fixed at 1.9, D/k_B = –0.35 cm^{-1}) and an S = 8 ground state (g = 1.8, D/k_B = –0.24 cm^{-1}), respectively. Neither complex could be reasonably fit to an S = 9 ground state as suggested by the $\chi_M T$ data. However, since this model assumes that only the ground state is being populated, these results are not completely unexpected in light of the $\chi_M T$ fits which clearly indicate the presence of low-lying excited states.

Alternating-current (AC) magnetic susceptibility studies were also conducted to determine the potential-energy barrier for reversal of the magnetization. Both complexes show a frequency-dependent out-of-phase AC signal (χ_M'') in the 5–1.8 K temperature range as shown in Figure S3 (complex **1**) and Figure 4 (complex **2**). The lowest frequency data (10 Hz) were plotted as $\chi_M T$ vs. T and extrapolated to 0 K in order to further confirm the ground-state spin of the complex. For **1**, the extrapolation gave a value of 32 cm^3 mol^{-1} K, which lies between the spin-only values for S = 7 (28 cm^3 mol^{-1} K) and S = 8 (36 cm^3 mol^{-1} K) ground states. For **2**, however, a value of 34 cm^3 mol^{-1} K was calculated, which supports an S = 8 ground state as indicated by the reduced magnetization data.

Though the maximum χ_M'' values for **1** are not observed above the 1.8 K lower limit of the instrument, those for **2** begin to emerge around 2.75 K at the highest AC frequency measured (997 Hz). By using the maximum at each frequency from 997 to 50 Hz, the data were fit to the Arrhenius equation $\tau = \tau_0 e^{-E_a/(kT)}$, where E_a is the activation energy, k is Boltzman's constant, τ is the relaxation time, and τ_0 is the preexponential factor. A plot of ln(τ) vs. $1/T$ (Figure 5) gave a linear correlation from which the E_a value was calculated and found to be 15.8 cm^{-1}. This agrees with the theoretical barrier ($-DS_z^2$) of 15.4 cm^{-1} calculated from the parameters S = 8 and D = –0.24 cm^{-1}, which were obtained from the field-dependent magnetization fitting of **2**.

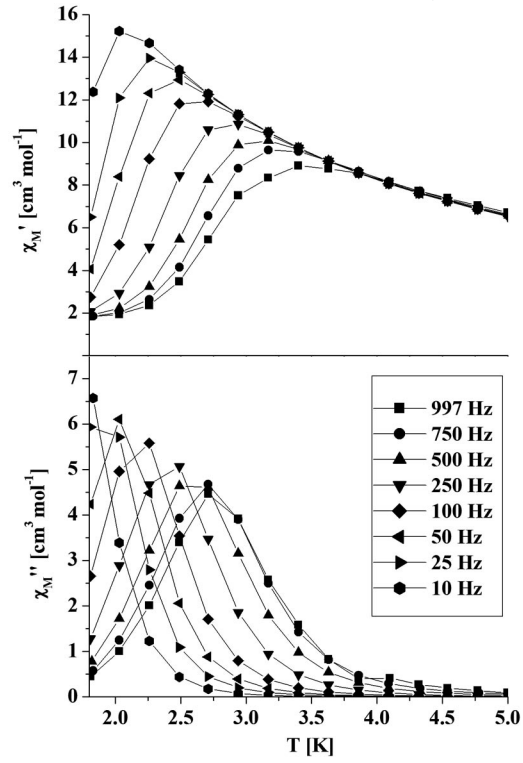

Figure 4. In-phase (χ_M') and out-of-phase (χ_M'') AC susceptibility for **2**.

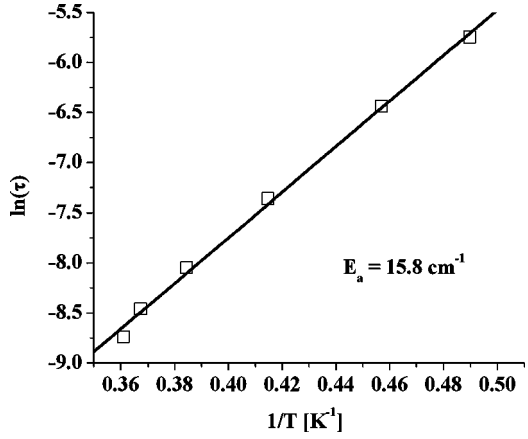

Figure 5. Arrhenius plot of out-of-phase AC susceptibility for **2**.

Conclusions

Two new ferromagnetic [$Mn^{II}_2Mn^{III}_2$] dicubane complexes have been synthesized and characterized. Fitting of the DC magnetic data along with analysis of the low-frequency AC data suggests an S = 7 or 8 ground state for **1** and a likely S = 8 ground state for **2**. The presence of a significant frequency-dependent out-of-phase signal in the

AC susceptibility further confirms that complexes **1** and **2** are the first ferrocene-substituted SMMs known to date.

Electrochemical studies are currently being carried out to determine the redox properties of **1** and **2** in order to help gauge the feasibility of oxidizing the Fc moieties on the Mn SMMs. Preliminary results suggest that the desired Fc^+ analogs of **1** and **2** should be accessible (either chemically or electrochemically) but the effect that the resulting S = 1/2 Fe^{III} ions might have on the ferromagnetic $[Mn_4]$ core is still unknown. Hence, modification of the ferrocenecarboxylate ligand is underway in order to facilitate the oxidation process and attempt to lessen any adverse effects the Fc^+ unpaired electron might have on the overall structural integrity and magnetic properties of the SMM.

Experimental Section

General: All reactions were performed under aerobic conditions. The reagents ferrocenecarboxylic acid ($FcCO_2H$), *N*-methyldiethanolamine (H_2mdea), *N*-butyldiethanolamine (H_2bdea), manganese(II) acetate tetrahydrate, and triethylamine (Et_3N) were purchased from Sigma Aldrich and used without further purification.

$[Mn_4(O_2CFc)_4(MdeaH)_2(Mdea)_2]\cdot 4MeCN$ (1): Excess Et_3N and $Mn(O_2CMe)_2\cdot 4H_2O$ (128 mg, 0.52 mmol) was added to a solution of $FcCO_2H$ (300 mg, 1.3 mmol) in MeCN (75 mL). $MdeaH_2$ (0.2 mL, 1.6 mmol) was added dropwise to the suspension, which was allowed to reflux for 1 h. The resulting dark orange-brown solution was cooled to room temperature and filtered by gravity. X-ray quality crystals were obtained by Et_2O vapor diffusion after 3–5 d in 33% yield (77 mg). $C_{66}H_{82}Fe_4Mn_4N_4O_{16}$ (1630.51): calcd. C 48.62, H 5.07, N 3.44; found C 46.48, H 5.06, N 3.68. Selected FT-IR data (KBr): $\tilde{\nu}$ = 3433 (s, br.), 2955 (w), 1605 (w), 1587 (w), 1545 (s), 1470 (s), 1389 (s), 1358 (s), 1321 (m), 1093 (m), 1070 (m, br.), 912 (w), 515 (m) cm^{-1}.

$[Mn_4(O_2CFc)_4(bdeaH)_2(bdea)_2]\cdot 2$ MeCN (2): Prepared according to the same procedure as described for complex **1** except by adding $BdeaH_2$ (0.2 mL, 1.6 mmol) in place of $MdeaH_2$. X-ray quality crystals obtained from Et_2O diffusion of the MeCN solution after 3–5 d in 48% yield (115 mg). $C_{76}H_{106}Fe_4Mn_4N_4O_{16}$ (1774.80): calcd. C 51.43, H 6.02, N 3.16; found C 51.07, H 6.06, N 3.13. Selected FT-IR data (KBr): $\tilde{\nu}$ = 3442 (m, br.), 3095 (w), 2956 (m), 2860 (m), 1606 (m), 1549 (m), 1470 (s), 1389 (s), 1358 (s), 1321 (s), 1178 (w), 1105 (m), 1076 (m), 910 (w), 766 (w), 513 (m) cm^{-1}.

Physical Techniques: FT-IR spectra were collected by using a Thermo-Nicolet Avatar series spectrometer. Elemental analysis was performed by NuMega Resonance Labs (San Diego, CA). Note: The formulas listed for the elemental analysis of **1** and **2** do not include solvate molecules as they are lost upon removal from the mother liquor. The DC magnetic susceptibility data were collected with a Quantum Design MPMS-5 magnetometer using a 5.5 Tesla magnet. Microcrystalline samples were restrained with eicosane to prevent torquing. Diamagnetic corrections of magnetic susceptibility data were made by employing Pascal's constants.

X-ray Crystallography: Crystals were mounted on a CryoLoop© with Paratone-N© oil. Diffraction intensity data were collected at 100(2) K with a Bruker Smart Apex CCD diffractometer with Mo-K_α radiation, integrated by using the Bruker SAINT software program, and corrected for absorption by using the Bruker SADABS program. Crystallographic data and refinement parameters for complexes **1** and **2** are given in Table S1. The structures of complexes **1** and **2** were solved by direct methods (SIR-2004 and DIRDIF-99, respectively), developed by successive difference Fourier syntheses, and refined by full-matrix least squares on all F^2 data. All non-hydrogen atoms were refined anisotropically by full-matrix least squares (SHELXL-97). All hydrogen atoms were placed by using a riding model, and their positions were constrained relative to their parent atoms by using the appropriate HFIX command in SHELXL-97. Acetonitrile solvate molecules were modeled and refined anisotropically in both complexes. A positionally disordered *N*-methyldiethanolamine ligand in **1** was modeled in two parts (Part 1 = C2, C4, C5; Part 2 = C2A, C4A, C5A) and refined to a final occupancy of 68% for Part 1. CCDC-723439 (for **1**) and CCDC-723440 (for **2**) contain the supplementary crystallographic data for this paper. These data can be obtained free of charge from The Cambridge Crystallographic Data Centre via www.ccdc.cam.ac.uk/data_request/cif.

Supporting Information (see footnote on the first page of this article): Crystallographic details, bond valence sum analyses, ORTEP of **1**, additional DC and AC magnetic data for **1**.

Acknowledgments

This work was supported by the National Science Foundation.

[1] a) S. M. J. Aubin, M. W. Wemple, D. M. Adams, H. L. Tsai, G. Christou, D. N. Hendrickson, *J. Am. Chem. Soc.* **1996**, *118*, 7746–7754; b) R. Sessoli, H. L. Tsai, A. R. Schake, S. Wang, J. B. Vincent, K. Folting, D. Gatteschi, G. Christou, D. N. Hendrickson, *J. Am. Chem. Soc.* **1993**, *115*, 1804–1816; c) R. Sessoli, D. Gatteschi, A. Caneschi, M. A. Novak, *Nature* **1993**, *365*, 141–143.

[2] a) G. Christou, D. Gatteschi, D. N. Hendrickson, R. Sessoli, *Mrs Bull.* **2000**, *25*, 66–71; b) D. Gatteschi, R. Sessoli, *Angew. Chem. Int. Ed.* **2003**, *42*, 268–297.

[3] D. N. Hendrickson, E. C. Yang, R. M. Isidro, C. Kirman, J. Lawrence, R. S. Edwards, S. Hill, A. Yamaguchi, H. Ishimoto, W. Wernsdorfer, C. Ramsey, N. Dalal, M. M. Olmstead, *Polyhedron* **2005**, *24*, 2280–2283.

[4] W. Wernsdorfer, N. Allaga-Alcalde, D. N. Hendrickson, G. Christou, *Nature* **2002**, *416*, 406–409.

[5] A. Masello, M. Murugesu, K. A. Abboud, G. Christou, *Polyhedron* **2007**, *26*, 2276–2280.

[6] C. C. Beedle, C. J. Stephenson, K. J. Heroux, W. Wernsdorfer, D. N. Hendrickson, *Inorg. Chem.* **2008**, *47*, 10798–10800.

[7] S. J. Shah, C. M. Ramsey, K. J. Heroux, A. G. DiPasquale, N. S. Dalal, A. L. Rheingold, E. del Barco, D. N. Hendrickson, *Inorg. Chem.* **2008**, *47*, 9569–9582.

[8] D. Foguet-Albiol, T. A. O'Brien, W. Wernsdorfer, B. Moulton, M. J. Zaworotko, K. A. Abboud, G. Christou, *Angew. Chem. Int. Ed.* **2005**, *44*, 897–901.

[9] A. M. Ako, V. Mereacre, I. J. Hewitt, R. Clerac, L. Lecren, C. E. Anson, A. K. Powell, *J. Mater. Chem.* **2006**, *16*, 2579–2586.

[10] S. J. Shah, C. M. Ramsey, K. J. Heroux, J. R. O'Brien, A. G. DiPasquale, A. L. Rheingold, E. del Barco, D. N. Hendrickson, *Inorg. Chem.* **2008**, *47*, 6245–6253.

Received: June 9, 2009
Published Online: July 16, 2009

